Optica Applicata, Vol. L, No. 1, 2020
DOI: 10.37190/oa200110

Depth dependent X-ray diffraction of porous anodic alumina films filled with cubic $YAlO_3:Tb^{3+}$ matrix

Jarosław SERAFIŃCZUK[1, 2*], Łukasz PAWLACZYK[1], Artur PODHORODECKI[3], Nikolai GAPONENKO[4], Igor MOLCHAN[5], George THOMPSON[5]

[1]Department of Nanometrology, Wrocław University of Science and Technology, Janiszewskiego 11/17, 50-372 Wrocław, Poland

[2]Łukasiewicz Research Network – PORT Polish Center for Technology Development, Stabłowicka 147, 54-066 Wrocław, Poland

[3]Department of Experimental Physics, Faculty of Fundamental Problems of Technology, Wrocław University of Science and Technology, St. Wyspiańskiego 27, 50-370 Wrocław, Poland

[4]Belarusian State University of Informatics and Radioelectronics, 6 P. Browki St., 220013 Minsk, Belarus

[5]Corrosion and Protection Centre, School of Materials, The University of Manchester, The Mill, Sackville St., Manchester, M13 9PL, UK

[*]Corresponding author: jaroslaw.serafinczuk@pwr.edu.pl

The presented paper deals with the measurement methodologies of the structural properties of porous anodic alumina (PAA) films filled with $YAlO_3:Tb^{3+}$ composite using X-ray diffraction, atomic force microscopy and scanning electron microscopy. It shows that the deposited material does not uniformly fill the porous volume of the anodic alumina film and the part of it forms a thick layer on the PAA surface. The aim of this work is to show the differences in the XRD response obtained at different angles of incidence of the excitation beam for the PAA/$YAlO_3:Tb^{3+}$ system. Furthermore, this simple approach enables separation of the signal from both regions on the surface and inside the PAA pores, providing more accurate data interpretation. It reveals that the crystallization of the material on the PAA surface and within the pores is different.

Keywords: PAA, X-ray diffraction, AFM, SEM, crystallization.

1. Introduction

Self-organized porous structures are promising materials for photonics applications due to their high surface areas and the possibility of using the photonic effect for controlling the emission properties of different species introduced within the pores [1]. Moreover, the use of a porous structure as a patterned substrate for deposition of other materials can add new properties to the materials [2, 3]. Furthermore, a quasi-continuous, nanotex-

tured, 1 μm thickness $YAlO_3$ film was formed in porous anodic alumina (PAA) [4, 5] which is complicated employing other approaches.

Examination of PAA with material embedded in the pores may not be straightforward due to the formation of the material both at the top of the substrate and within the pores. Consequently, the material may be present in at least two different phases due to the different growth conditions. This is even more complicated for pseudo-binary compounds such as yttria-aluminum composite, which are known to exist in three different phases, namely yttrium aluminum garnet (YAG, $Y_3Al_5O_{12}$), yttrium aluminum perovskite (YAP, $YAlO_3$) [6] and yttrium aluminum monoclinic (YAM, $Y_4Al_2O_9$). Further, more than one form of $YAlO_3$, *e.g.* hexagonal, cubic and amorphous, can be obtained under low temperature annealing conditions [7]. In most cases, one material may be present as a combination of several phases. In this case, the situation is even more complicated since an additional, native oxide form may be present in the walls of the substrate [8, 9]. Additionally, doping with lanthanides can also influence the structural properties of the material [10].

One of the well-known techniques that is sensitive to crystalline phases is XRD. However, it is important to interpret precisely the XRD results since the proper interpretation of the phase contents will have important consequences in interpreting the optical properties. For example, the optical properties of lanthanide ions strongly depend on their local environment, *e.g.* present in a crystalline phase.

Thus, the aim of this work is to analyze structural properties of PAA/$YAlO_3$:Tb^{3+} samples obtained at three different Tb^{3+} concentrations, including the complex character of the material.

2. Experiment

Samples have been fabricated by co-precipitation in PAA grown on silicon and annealed at 1000°C. More details regarding the samples preparation can be found in our recent paper [4].

XRD spectra were obtained using a PHILIPS MRD diffractometer supported by the parallel beam optics and $CuK_{\alpha 1}$ = 1.540597 Å radiation source. Theta-2theta scans and 2theta with a constant incident beam were performed. AFM images were collected using a VS microscope with the NanoScope V controller (Veeco Instruments) and a silicon tip operating in the tapping mode.

A Zeiss Ultra-55 scanning electron microscope (SEM), equipped with backscattered electron detection (BSDE) mode and energy dispersive X-ray (EDX) detectors, was employed for examination of the cross-section and chemical compositions of the samples. An acceleration voltage of 2 kV was used for recording the backscattered electron images with high *Z*-contrast. For examination of the cross-sections, the samples were fractured immediately prior to placing in the SEM chamber to minimize contamination that is crucial for imaging of non-conductive materials using BSDE. The acceleration voltage was increased to 8 kV for EDX characterization. EDX was employed to determine the concentration of Tb in the samples. Each sample was analyzed six times.

The analysis was undertaken from the top of $YAlO_3$ layer covering PAA. Thanks to it, we achieved the minimum influence of the PAA matrix. We also assumed that the $YAlO_3$ composition is the same in the pores. The diameter and penetration depth of the electron beam in $YAlO_3$ at an accelerating voltage of 8 kV are approximately 500 and 600 nm, respectively. This suggested that the contribution of the PAA matrix to the elemental composition is insignificant [4].

3. Results and discussion

First, three PAA:$YAlO_3$:Tb^{3+} samples, obtained with three different Tb^{3+} concentrations (0.22, 0.87 and 2.11 at.%), were investigated using AFM and SEM. Figure 1 shows the surface topography of the selected sample obtained by AFM. It is evident in Fig. 1**a** that the material does not completely cover the macroscopic surface of the PAA film; the material is cracked, forming approximately continuous areas of approximately 4 × 4 µm dimensions and 1 µm thickness. Open pores of the anodic alumina film may be observed in the individual cracks (Fig. 1**b**). However, due to the limited resolution of AFM, the granular structure of the materials deposited at the surface is not evident. Similar images have been obtained for all other samples and no influence of Tb^{3+} concentration on the surface morphology is evident. Moreover, Fig. 1**c** shows a digital image of investigated sample at 270 nm excitation, revealing strong green

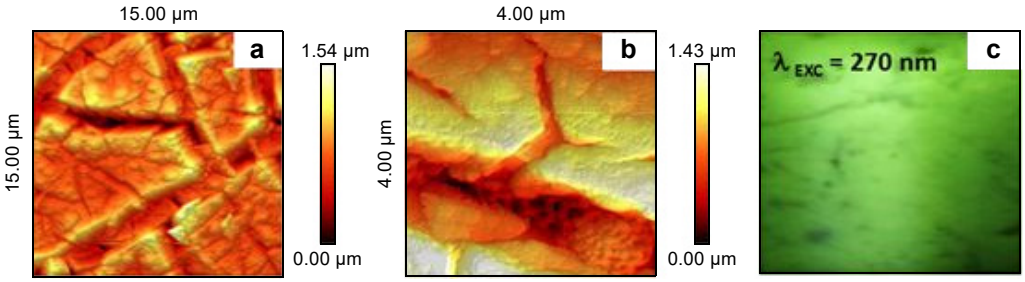

Fig. 1. AFM images of the surface of the PAA/$YAlO_3$:Tb^{3+} sample with 0.87 at.% Tb^{3+} (**a**, **b**), and digital image of the sample surface at an excitation wavelength of 270 nm (**c**).

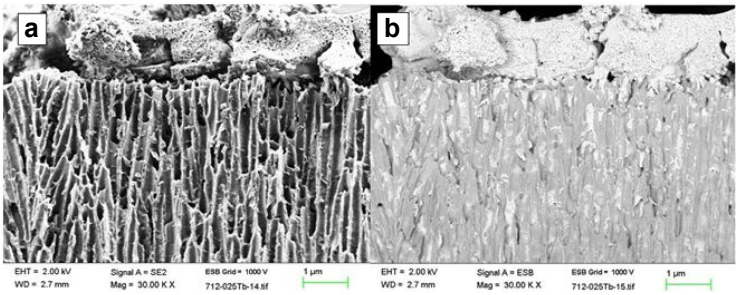

Fig. 2. Scanning electron micrographs of the PAA/$YAlO_3$:Tb^{3+} sample with 0.87 at.% Tb^{3+}: SEM image (**a**), and EDX image (**b**).

emission from Tb^{3+} ions. Detailed investigations of optical properties of such materials have been already discussed elsewhere [4, 5].

In order to gain further insight into the morphology of the samples, the cross-sections of the samples were examined by SEM. Figure 2 shows the scanning electron micrographs for the PAA/$YAlO_3$:Tb^{3+} sample with 0.87 at.% Tb^{3+}, revealing that the pores are partially filled with the material. Considering the much greater thickness of the PAA film than the layer of material deposited on the film surface, we should expect a significant contribution from the material confined within the pores to the macroscopic response of the sample. Moreover, it is suspected that crystallization of the yttrium-alumina composite at the surface and inside the pores takes place in a different way. Furthermore, doping of Tb^{3+} ions in the pores may occur in a variety of ways which influences the crystallization of $YAlO_3$ in the pores and on the sample surface. Unfortunately, this effect of different crystallization types cannot be seen from the microscopic images. Therefore, the X-ray diffraction method has been used to study phase contents.

XRD is one of the basic methods which allows determination of the structural parameters of a material, calculation of particle size and phase identification. One of the basic measurement methods in XRD is the so-called theta-2theta scan, which involves measuring the diffraction pattern from the sample surface while changing the angle of incidence and diffraction of the X-ray beam. The method enables to obtain reflections from all crystal planes of the measured sample which are parallel to the surface plane of the sample. The application of this method in this case is not proper because the information about phase contents in $YAlO_3$ is received from various locations, including the surface layer and pore volume of the anodic film – Fig. 3**a**. Thus, the measurements that separate information from the bulk and the surface of the sample are required. This may be realized by measurement at a constant small angle of incidence of the X-ray

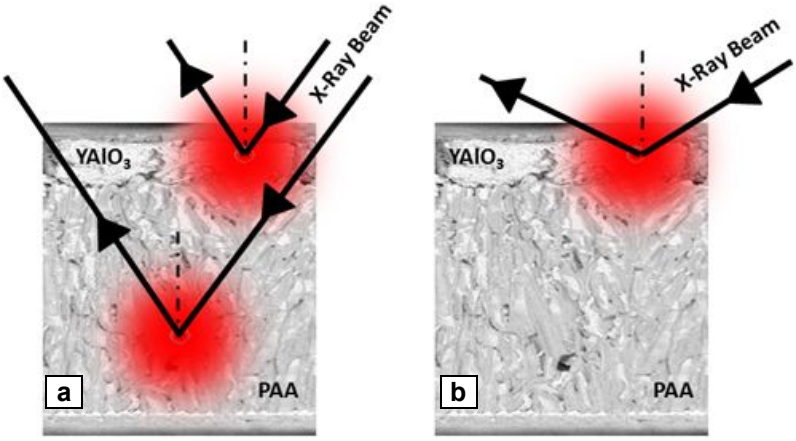

Fig. 3. Diagram of X-ray beams to scans: theta-2theta (**a**), and 2theta with constant incidence beam (**b**); the area of X-ray beam penetrating the structure was indicated.

beam to the sample (<7°, typically 4°) [11]. At low angle, the beam slips over the surface and does not penetrate deeply into the sample, thus probing the near-surface region of the sample – Fig. 3**b**. In theta-2theta measuring mode, the depth of penetration of the X-ray beam is variable and depends on the angle of incidence. For the initial value, *i.e.* 5° is 4.60 μm, and for the end value, *i.e.* 55° is 43.24 μm. For constant angle of incidence equal to 4° we have constant penetration depth 3.68 μm.

The two types of measurement that have been performed, including theta-2theta scan and 2theta scan, employ various and constant angle of incidence of the beam to the sample, respectively. Figure 4 shows the diffraction curves for both cases. Significant differences in XRD signals can be observed for all samples for both XRD configurations. This could be due to the fact that in one case we probe mainly the top layer of $YAlO_3$ materials, while in the second case we average the signal from material in two regions: at the PAA near-surface region only and averaged over the surface and porous volume.

The main differences are clearly distinguished by comparing the reflections between 50° and 60° and the reflections around 30°. In the theta-2theta scans, these reflections have much reduced intensity than the 2theta scans. In the 2theta scans, the reflections related to Al_2O_3, located near 70°, are weak. This confirms that for the 2theta scan with a small and constant angle of incidence, the X-ray beam slightly penetrates into the sample, thus collecting information from the material located mainly on the surface of the PAA film. Reflections of Al_2O_3 on these scans are less intense. For the theta-2theta scan, the angle of incidence of the X-ray beam to the sample varies

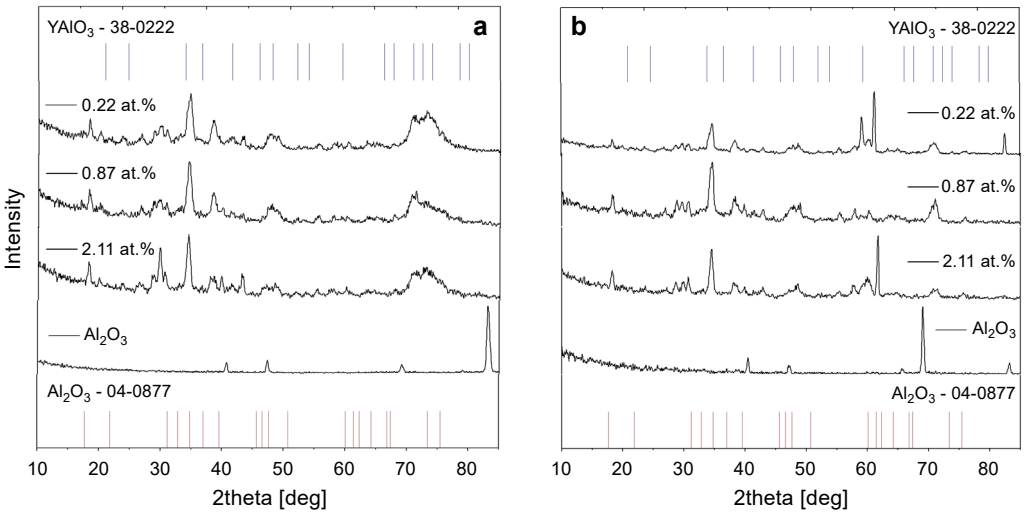

Fig. 4. XRD Spectra of the measured samples annealed with different concentration of Tb^{3+} ions and the XRD spectra of the Al_2O_3 (JCPDS Card No. 04-0877) matrix without the $YAlO_3$ composite. Other unmarked peaks come from $YAlO_3$ particles (JCPDS Card No. 38-0222); theta-2theta scan mode (**a**), and 2theta scan mode (**b**).

from 5° to 55°; the larger the angle of incidence, the greater the penetration depth of the X-ray beam into the sample. Thus, the presented diffraction patterns display relatively intense reflections from the alumina matrix.

In addition, for both types of scans and for selected reflections, the average sizes of the crystallites were determined. For this calculation, the Scherrer equation [12] was used

$$d = \frac{0.9\lambda}{\beta \cos\theta}$$

where λ is the wavelength of the X-ray radiation, β is the full width at half maximum of the peak by which the crystallite size is determined and θ is the Bragg angle of the concerned diffraction peak.

The average dimensions of the crystallites in the surface layer are much larger than those in the pores. The average pore diameter in the PAA layer is 150 nm. For the sample with 0.87 at.% of Tb^{3+}, the peak that was located at position 32.8 the average crystallite size were 306 Å, and for crystallites which were inside the alumina matrix were 240 Å. The uncertainty of the Scherrer equation depends on the value of β and for this range of crystallite size is 5% [13]. Significantly, it was revealed from Scherrer analysis that the size of the $YAlO_3$ grains depends on Tb^{3+} concentration. For $YAlO_3$ peak centered at 32.8°, the crystallite size determined for the 2theta scan mode increases in the order 263 Å for 0.22 at.% < 321 Å for 0.87 at.% < 418 Å for 2.11 at.%. For theta-2theta scans the order is as follows: 187 Å for 0.22 at.% < 234 Å for 0.87 at.% < 373 Å for 2.11 at.% (Fig. 5). It can be concluded that the crystallite sizes of $YAlO_3$ located on the surface region of the samples are larger than those located in the pores of anodic alumina. From this it follows that the size of the crystallizing particles depends not only on the Tb^{3+} ion concentration, but also the on areas in which crystallization occurs. Such areas include the porous space confined within the walls of the anodic alumina cell or the free space outside the pores.

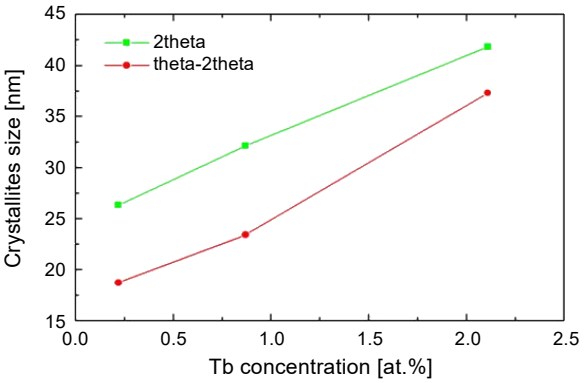

Fig. 5. Crystallite size of $YAlO_3$ *vs*. concentration of Tb^{3+} ions.

For the same type of scan, differences are evident between the intensities of a particular reflection. For the theta-2theta scans, the intensity of the reflection at 17° increases with increase of Tb^{3+} concentration from 110 cps for 0.22 at.% to 117 cps for 0.87 at.% and 2.11 at.%. This tendency is also evident for the 2theta scans, where for the same $YAlO_3$ reflections, the intensity increases from 109 cps for 0.22 at.% to 123 cps for 2.11 at.%; however, the intensity for the sample with 0.87 at.% Tb^{3+} is 128 cps. This difference is consistent with the thickness of $YAlO_3$ composite deposited on the sample surface.

4. Conclusion

We have shown in the present study that spatially different information about the PAA/$YAlO_3$ structure may be generated, depending on the type of XRD scan. The 2theta scan at a constant, relatively small angle of incidence of the X-ray beam (typically 4°) provides information about the surface layer due to the shallow penetration of the sample by the X-ray beam. Conversely, for the theta-2theta scan with the angle of incidence of the X-ray beam varying from 5° to 55° provides information from the bulk of the sample due to the relatively deep penetration. It was revealed by employing a combination of the two types of scans applied to the PAA/$YAlO_3$:Tb^{3+} composite structure that *i*) crystallites size in the $YAlO_3$:Tb^{3+} surface layer is larger than that in the pores of PAA, and *ii*) the increasing concentration of Tb^{3+} ions in $YAlO_3$ causes generation of larger $YAlO_3$ crystallites.

Acknowledgments – This work was supported by the National Center of Science OPUS 13 Grant No. 2017/25/B/ST7/01203, as well as a Statutory Grant of Department of Nanometrology of WrUST.

References

[1] Wittmann H.F., Grüner J., Friend R.H., Spencer G.W.C., Moratti S.C., Holmes A.B., *Microcavity effect in a single-layer polymer light-emitting diode*, Advanced Materials **7**(6), 1995, pp. 541–544, DOI: 10.1002/adma.19950070604.

[2] Podhorodecki A., Gaponenko N.V., Banski M., Rudenko M.V., Khoroshko L.S., Sieradzki A., Misiewicz J., *Green emission from barium-strontium titanate matrix introduced into nano-porous anodic alumina*, Optical Materials **34**(9), 2012, pp. 1570–1574, DOI: 10.1016/j.optmat.2012.03.025.

[3] Gaponenko N.V., Kortov V.S., Rudenko M.V., Pustovarov V.A., Zvonarev S.V., Slesarev A.I., Molchan I.S., Thompson G.E., Khoroshko L.S., Prislopskii S.Ya., *Inhomogeneous nanostructured honeycomb optical media for enhanced cathodo- and under-x-ray luminescence*, Journal of Applied Physics **111**(10), 2012, article 103101, DOI: 10.1063/1.4717740.

[4] Podhorodecki A., Gaponenko N., Zatryb G., Molchan I.S., Motyka M., Serafinczuk J., Golacki L., Khoroshko L.S., Misiewicz J., Thompson G.E., *Ion–ion interaction in two-dimensional nanoporous alumina filled with cubic $YAlO_3$: Tb^{3+} matrix*, Journal of Physics D: Applied Physics **46**(35), 2013, article 355302.

[5] Liu, B. Shi J., Wang Q., Tang H., Liu J., Zhao H., Li D., Liu J., Xu X., Wang Z., Xu J., *Crystal growth, polarized spectroscopy and Judd–Ofelt analysis of Tb:$YAlO_3$*, Spectrochimica Acta Part A: Molecular and Biomolecular Spectroscopy **200**, 2018, pp. 58–62, DOI: 10.1016/j.saa.2018.04.006.

[6] GOLACKI L.W., GAPONENKO N.V., KHOROSHKO L.S., ASHARIF A.M., MISIEWICZ J., PODHORODECKI A., *Thermal Tb emission quenching in $YAlO_3$ matrix embedded in porous anodic alumina*, Optical Materials **37**, 2014, pp. 200–203, DOI: 10.1016/j.optmat.2014.05.024.

[7] PODHORODECKI A., BANSKI M., MISIEWICZ J., SERAFINCZUK J., GAPONENKO N.V., *Influence of annealing on excitation of terbium luminescence in $YAlO_3$ films deposited onto porous anodic alumina*, Journal of The Electrochemical Society **157**(6), 2010, pp. H628–H632.

[8] YAMAGUCHI O., TAKEOKA K., HIROTA K., TAKANO H., HAYASHIDA A., *Formation of alkoxy-derived yttrium aluminium oxides*, Journal of Materials Science **27**, 1992, pp. 1261–1264, DOI: 10.1007/BF01142034.

[9] TANNER P.A., LAW P.T., WONG K.L., FU L., *Preformed sol-gel synthesis and characterization of $YAlO_3$*, Journal of Materials Science **38**, 2003, pp. 4857–4861, DOI: 10.1023/B:JMSC.0000004405.52574.37.

[10] PODHORODECKI A., ZATRYB G., MISIEWICZ J., DOMARADZKI J., KACZMAREK D., BORKOWSKA A., *Influence of annealing on europium photoexcitation doped into nanocrystalline titania film prepared by magnetron sputtering*, Journal of The Electrochemical Society **156**(3), 2009, pp. H214–H219.

[11] SIMEONE D., BALDINOZZI G., GOSSET D., LE CAER S., BÉRAR J.-F., *Grazing incidence X-ray diffraction for the study of polycrystalline layers*, Thin Solid Films **530**, 2013, pp. 9–13, DOI: 10.1016/j.tsf.2012.07.068.

[12] SIMEONE D., BALDINOZZI G., GOSSET D., ZALCZER G., BÉRAR J.-F., *Rietveld refinements performed on mesoporous ceria layers at grazing incidence*, Journal of Applied Crystallography **44**(6), 2011, pp. 1205–1210, DOI: 10.1107/S0021889811042294.

[13] ALEXANDER L., KLUG H.P., *Determination of crystallite size with the X-ray spectrometer*, Journal of Applied Physics **21**(2), 1950, pp. 137–142, DOI: 10.1063/1.1699612.

Received February 8, 2019
in revised form March 6, 2019